

Magnetically tunable Feshbach resonances in Li+Er

Maykel L. González-Martínez^{1,*} and Piotr S. Żuchowski^{2,†}

¹Laboratoire Aimé Cotton, CNRS, Université Paris-Sud, ENS Cachan, Bâtiment 505, Campus d'Orsay, 91405 Orsay, France

²Institute of Physics, Faculty of Physics, Astronomy and Informatics, Nicolaus Copernicus University,
ul. Grudziadzka 5/7, 87-100 Toruń, Poland

(Received 8 June 2015; published 24 August 2015)

We explore the magnetic Feshbach spectra of ultracold ground-state Li+Er systems. Our calculations predict many tunable resonances at fields below 1000 G that could be stably tuned in ultracold experiments. We show that Li+Er spectra are much less congested than those of systems involving heavier highly magnetic atoms and exhibit nonchaotic properties. These features would facilitate identifying and addressing individual resonances. We derive a simple model for the mass-scaling shifting of low-field resonances that may simplify designing experiments with different Er bosonic isotopes. Our work establishes Li+Er as very promising systems for quantum simulation, precision measurements and the formation of polar paramagnetic molecules.

DOI: [10.1103/PhysRevA.92.022708](https://doi.org/10.1103/PhysRevA.92.022708)

PACS number(s): 34.50.Cx, 37.10.-x, 67.85.-d

I. INTRODUCTION

Ultracold species make it possible to build state-selected quantum systems with controllable interactions, which open the door to exploring fascinating phenomena. Among their many applications [1,2], ultracold systems can be used as quantum simulators [3,4], to study condensed-matter physics [5–7] and quantum-controlled chemistry [8–10], to develop quantum information devices [11,12], and for ultraprecise spectroscopy [13–15].

Tunable Feshbach resonances [16] are powerful tools to control the interaction and scattering properties of ultracold species, making many of these applications possible. Moreover, they are essential in the most successful scheme to date to produce ultracold molecules: The magneto- or photoassociation of ultracold atoms [17–19] followed by coherent [20–23] transfer of the created molecules to their rovibrational ground states. Having the possibility to address and tune across selected Feshbach resonances is thus key in ultracold experiments.

Recent advances in cooling highly-magnetic atoms such as Cr(⁷S) [24,25], Dy(⁵I) [26,27], and Er(³H) [28,29] open exciting opportunities for tunability and control [30]. The interaction between these atoms, however, leads to highly congested Feshbach spectra with many overlapping resonances per gauss [31–33]. This makes it impractical to assign quantum labels to individual resonances and may be a challenge to interaction “tailoring” and molecule formation.

In this paper, we study magnetic *s*-wave Feshbach resonances in binary mixtures of ground-state Li atoms and bosonic Er isotopes. The Li+Er system may be especially appealing for ultracold experiments in optical lattices: Dipolar species with tunable interactions are key to studying the effects of long-range anisotropies, quantum magnetism, disorder, and quantum collective behavior [10,25,34–36]. Very importantly, such Feshbach resonances may be used for magnetoassociation of LiEr molecules, starting from ground-state atoms in order to avoid limiting background losses [37]. Ground-

state LiEr molecules have both magnetic and electric dipole moments [38], and may be controlled with applied electric and magnetic fields, which further enhances their applicability [4,34,39,40]. In addition, Er is a heavy atom, thus ultracold LiEr may be used to study the time variation of fundamental constants [13,14], while the extreme mass imbalance in the system makes it specially well suited for exploring Efimov physics [41].

II. THEORY

We carried out coupled-channel calculations using the theory in Ref. [42]. The Hamiltonian can be written

$$\hat{\mathcal{H}} = -\frac{\hbar^2}{2\mu} R^{-1} \frac{d^2}{dR^2} R + \frac{\hbar^2 \hat{L}^2}{2\mu R^2} + \hat{\mathcal{H}}_{\text{Li}} + \hat{\mathcal{H}}_{\text{Er}} + \hat{\mathcal{U}}, \quad (1)$$

where μ is the reduced mass for the collision, R is the interatomic distance, and \hat{L} is the space-fixed operator for the end-over-end rotation. $\hat{\mathcal{H}}_{\text{Li}}$ and $\hat{\mathcal{H}}_{\text{Er}}$ describe the isolated atoms and are taken to be

$$\begin{aligned} \hat{\mathcal{H}}_{\text{Li}} &= b_{\text{F},\text{Li}} \hat{l}_{\text{Li}} \cdot \hat{s}_{\text{Li}} + (g_S \mu_B \hat{s}_{\text{Li}} - g_L \mu_N \hat{l}_{\text{Li}}) \cdot \mathbf{B}, \\ \hat{\mathcal{H}}_{\text{Er}} &= a_{\text{Er}}^{\text{so}} \hat{l}_{\text{Er}} \cdot \hat{s}_{\text{Er}} + (g'_L \mu_B \hat{l}_{\text{Er}} + g_S \mu_B \hat{s}_{\text{Er}}) \cdot \mathbf{B}. \end{aligned} \quad (2)$$

Here, \hat{l}_{Li} and \hat{s}_{Li} are the Li nuclear and electronic spin operators, while \hat{l}_{Er} and \hat{s}_{Er} denote the Er electronic orbital and spin operators (all bosonic Er isotopes have zero nuclear spin); \mathbf{B} is the external magnetic field. $g_S \approx 2$, $g_L \text{Li}$, and $g'_L \approx 1$ are the electron, Li nuclear and orbital *g* factors, while μ_B and μ_N are the Bohr and nuclear magnetons. The hyperfine coupling constants for ^{6,7}Li ($b_{\text{F},\text{Li}}$) and the nuclear *g* factors were taken from Refs. [43,44]. The spin-orbit coupling constant for Er, $a_{\text{Er}}^{\text{so}} = -1159.7215 \text{ hc cm}^{-1}$, was calculated from the splitting between the two lowest Er states, ³H₆ and ³H₅ [45], assuming Russel-Saunders coupling.

$\hat{\mathcal{U}}$ describes all interactions between the atoms and includes the electronic potential \hat{V} and the direct dipolar interaction between the atoms’ magnetic moments $\hat{\mathcal{H}}_{\text{dip}}$ [42]. Following Krems *et al.* [46], we decompose \hat{V} into functions with well-defined total spin S and space-fixed spin projection M_S , which are then expanded in Legendre polynomials—assuming that $l_{\text{Er}} = 5$ is conserved at all values of R . The

*maykel.gonzalez-martinez@u-psud.fr

†pzuch@fizyka.umk.pl

expansion coefficients, $\hat{V}_k^S(R)$ ($k = 0, 2, \dots, 2l_{\text{Er}}$), are linear combinations of the Born-Oppenheimer potentials [42,46]; these can be split into isotropic V_0^S and anisotropic $V_{k \neq 0}^S$ terms, the latter depending only on the energy *differences* between Born-Oppenheimer states.

III. RESULTS AND DISCUSSION

A. Interaction potentials

The interaction between Li(²S) and Er(³H) gives rise to twelve electronic states: six states corresponding to $|\Lambda| = 0, \dots, l_{\text{Er}}$ —the absolute value of the projection of the electronic orbital angular momentum onto the interatomic axis—for each S , $S_- = \frac{1}{2}$, and $S_+ = \frac{3}{2}$. We calculated the short-range interaction energies for all Li(²S)+Er(³H) states using the complete active space self-consistent field (CASSCF) method implemented in MOLPRO [47]. The active space includes 1s2s orbitals for Li and 4f6s6p orbitals for Er. We used the high-quality uncontracted aug-cc-pVQZ basis sets by Prascher *et al.* [48] for the Li atom. For Er, we used the quasirelativistic effective core potential by Dolg *et al.* [49] (ECP28MWB) for the first 28 electrons, with uncontracted s and p shells, to which we added h functions with exponent 0.45. The basis was augmented with extra diffused functions using the even-tempered scheme in MOLPRO [47]. The Li+Er states lie relatively close in energy and special care is needed to avoid their mixing. We start our *ab initio* calculations at large $R = 50a_0$, calculating the starting orbitals by merging those of the isolated atoms; this way, we obtain properly 22-fold degenerate states for Li+Er. In each following calculation, we take a step inwards in R and use the orbitals converged from the precedent geometry as starting orbitals. We obtain potentials corresponding to pure $\Lambda = 0, \dots \pm l_{\text{Er}}$ states by controlling the Λ quantum number of the molecule.

With this scheme, we get realistic short-range energy differences between all Li+Er potentials, and thus realistic anisotropies $V_{k \neq 0}^S$ from our CASSCF calculations. The active space, however, is not sufficiently large for describing the Li+Er dispersion accurately, which mainly affects the V_0^S isotropic terms. This can be fixed by noting that the dispersion interaction in analogous systems is relatively spin independent, with the spin-dependent exchange-dispersion energy being typically very small [50]. We thus assumed that the spin-independent dispersion interaction in Li+Er is similar to that in Li+Yb, which is supported by the similarity of their isotropic dispersion coefficients (1594 a.u. for Li+Yb [51] and 1508 a.u. for Li+Er; see calculation details below). We used the Heisenberg spin-exchange model [52–54] for the isotropic potentials, $V_0^S(R) = V_0(R) - 2J_0(R)\hat{s}_{\text{Li}} \cdot \hat{s}_{\text{Er}}$, and replaced the spin-independent term V_0 with the LiYb potential obtained by Zhang and coworkers using the best *ab initio* methods available [51]. The spin dependence in our Li+Er isotropic terms is obtained from $J_0 = -[V_0^{S+} - V_0^{S-}]/2S_+$, which depends on energy differences only and is thus recovered from our CASSCF calculations. We interpolated and extrapolated all V_k^S curves with the reproducing kernel Hilbert space (RKHS) approach of Ho and Rabitz [55]. Both V_0^S isotropic potentials were constrained at long range to have $C_{6,0} = 1508$ a.u., calculated from Tang's combination rule [56] with the values of

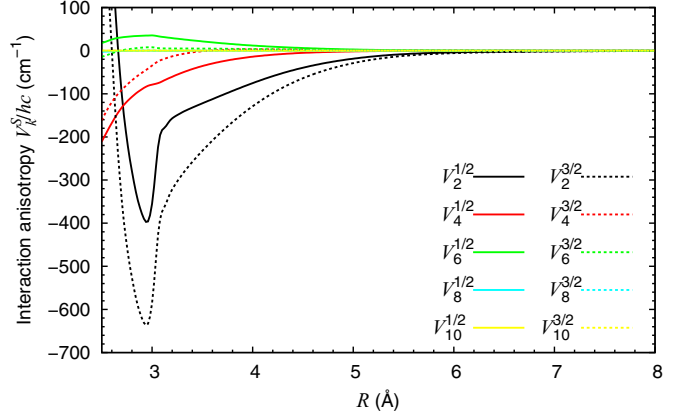


FIG. 1. (Color online) Calculated interaction anisotropies in Li+Er for low (solid) and high (dotted) total electronic spin. Line intensities decrease with increasing anisotropy order k .

the static polarizability and dispersion coefficients for Li₂ [57] and Er₂ [58]. The V_2^S anisotropies were constrained to have $C_{6,2} = 35.04$ a.u., calculated from $C_{6,0}$ and Er anisotropic and isotropic polarizabilities using an l -dependent ratio suitable for S+H systems (cf. Ref. [59]). We neglected the Van der Waals expansion in $V_{k \geq 4}^S$ terms, which decay faster than R^{-6} .

Figure 1 shows the CASSCF interaction anisotropies $V_{k \neq 0}^S$ for Li+Er. The magnitude of the spin-exchange interaction potential curves is qualitatively similar to recent calculations by Tomza on Li+Eu [40], for which the spin-exchange interaction near equilibrium was about 600 cm⁻¹. The fact that spin-exchange in this system is much smaller than for alkali dimers is explained by suppression due to the outermost 6s² shell of Er. The same mechanism reduces the anisotropies related to the electronic orbital angular momentum: they are on the order of few hundreds of cm⁻¹ near the Van der Waals minimum for V_2^S terms and orders of magnitude lower for higher-order anisotropies. The mechanism of suppression of L -anisotropy was found earlier by Krems and coworkers for the He + transition-metal systems [60] and for Yb+Tm by Buchachenko *et al.* [61]. This is in contrast to the Li+Yb(6s¹6p¹) system where the L -anisotropy is on the order of thousands of cm⁻¹ [37].

B. Magnetic Feshbach spectra

1. Resonances

We studied *s*-wave magnetic Feshbach resonances in the Li+Er systems using the MOLSCAT [62,63] and FIELD [64] packages. We used computational methods analogous to those in previous work on Li+Yb [37] and H+F [42]. The collision energy in our scattering calculations is fixed at $1k_{\text{B}}$ nK. Convergence in the partial-wave expansion was achieved with $L_{\text{max}} = 10$. We consider calculations with both atoms in their lowest Zeeman state.

Figure 2 shows the predicted magnetic field dependence of the Li+¹⁶⁶Er scattering length, depicting many Feshbach resonances of widths between 0.1 and 50 G that are very promising candidates for precise tuning and magnetoassociation. These resonances are immune to background losses since both species interact in their absolute ground state. We located

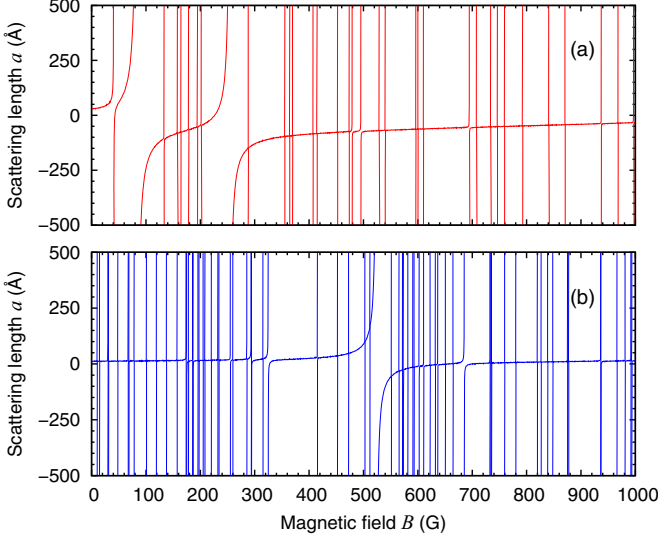


FIG. 2. (Color online) Magnetic field dependence of the scattering length $a(B)$ for ground-state collisions of ^{166}Er with (a) ^6Li , and (b) ^7Li .

35 (69) resonances below 1000 G for $^6\text{Li} + ^{166}\text{Er}$ ($^7\text{Li} + ^{166}\text{Er}$), and calculated mean densities of $\bar{\rho}_{^6\text{Li}} = 0.0364 \text{ G}^{-1}$ and $\bar{\rho}_{^7\text{Li}} = 0.0730 \text{ G}^{-1}$. The combination of light and heavy species yields a much wider rovibrational spacing than for a heavy+heavy system, hence Li+Er Feshbach spectra are much less congested than others involving highly magnetic atoms [31–33].

The couplings responsible for these resonances have been studied for analogous systems; cf. Refs. [37,42,46]. These involve orbital- and/or spin-anisotropies from the electronic potentials, with the widest resonances due to states dominated by low L quantum numbers. The general trends in our calculations support this reasoning. The widest resonances in Fig. 2 ($\Delta_B > 10$ G) correspond to states with over 55% and up to 45% compositions from $L = 0$ and 2, respectively, which are mainly coupled to the initial state by $V_{k=0,2}^S$ terms. An intermediate resonance “class” ($1 < \Delta_B < 5$ G) arises from states with over 30% composition of $L = 4$, and less than 15% of $L = 0$, involving V_4^S coupling terms. Narrower resonances are due to states with non-negligible higher-order orbital excitations of the complex, $L \geq 6$. Removing high-order anisotropies $V_{k>4}^S$, however, does not affect the overall resonance pattern since indirect mechanisms involving $V_{k\leq 4}^S$ terms also couple the resonant states to the continuum. The contribution from dipole-dipole interactions is very small compared to that of the potential terms and was found to be negligible, as for Li+Yb [37].

2. Spectra statistical properties

Studying the statistics of the calculated Feshbach spectra is key to unraveling their most general and robust properties. We performed an analysis similar to that of Frisch and coworkers [32], with added G tests and Bayes’ logarithmic likelihood ratio (LLR) [65] calculations.

Figure 3 shows the nearest-neighbor spacing (NNS) distribution and the number variance (Σ^2) for the calculated $^{6,7}\text{Li} + ^{166}\text{Er}$ Feshbach spectra; predictions from the Poisson

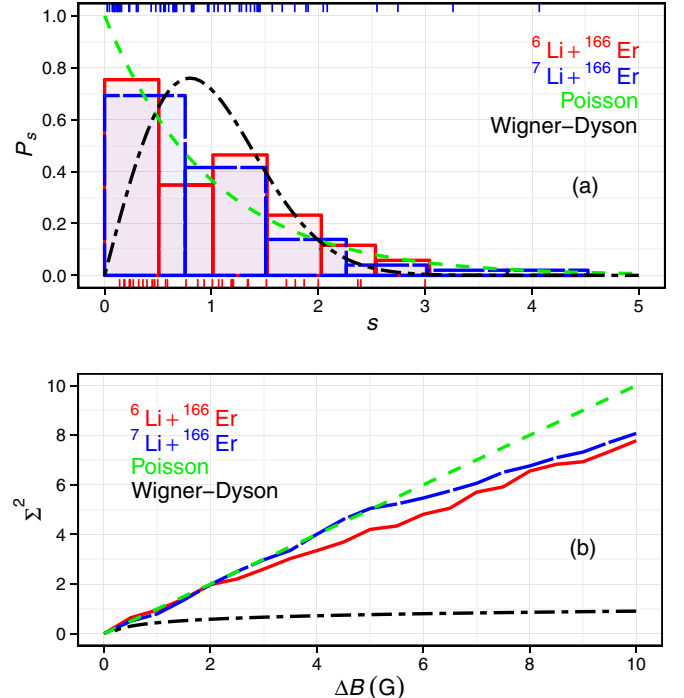


FIG. 3. (Color online) (a) Nearest-neighbor spacing distributions and (b) number variances for the $^6\text{Li} + ^{166}\text{Er}$ and $^7\text{Li} + ^{166}\text{Er}$ (solid red and long-dashed blue) spectra. Poisson (dashed green) and Wigner-Dyson (two-dashed black) curves are added for comparison.

and Wigner-Dyson models are added for comparison. In particular, Σ^2 measures fluctuations in the number of resonances per interval ΔB , averaged over each given spectrum. Our calculations span the range of magnetic fields of most experimental interest which include a limited number of resonances. Therefore, as ΔB increases, the fluctuations due to the finite size of the spectrum will affect the convergence of the calculated Σ^2 (as compared to an averaging over an infinite spectrum). Figure 3(b) shows the $^7\text{Li} + \text{Er}$ curve deviating from the Poisson model at roughly twice the value of ΔB than that of $^6\text{Li} + \text{Er}$. Given that $^7\text{Li} + \text{Er}$ has over twice the spectral density than $^6\text{Li} + \text{Er}$, the different ΔB “deviation thresholds” are most likely due to averaging over a finite size spectrum and not to an intrinsic difference between the two Li systems.

Table I summarizes all statistical tests performed and details on the fits to Brody NNS distributions. Unlike G tests, χ^2 statistics may become unstable for relatively scarce data and are mainly provided for comparison with related works; the χ^2 associated p -values were calculated from Monte Carlo simulations using 2000 replicates [66]. Bayes’ LLR is used to compare between two different hypothesis: that a given NNS distribution (x) arises from either a Poisson (H_P) or a Wigner-Dyson (H_{WD}) underlying distribution.

The statistical analysis indicate that Li+Er Feshbach spectra arise from weakly interacting levels exhibiting very low spectra rigidity and level repulsion, with Poisson-like models providing a significantly better description of the spectra. These are all characteristics of nonchaotic spectra and make it possible to identify and tune selected individual Feshbach resonances for interaction tailoring and/or magnetoassociation.

TABLE I. Summary of statistical tests and/or model fitting to Li+¹⁶⁶Er Feshbach spectra ($\tilde{\chi}$ and \tilde{G} are *reduced* quantities).

Lithium isotope	χ^2 test		G test		Bayes' LLR $\log [P(\mathbf{x} H_P)/P(\mathbf{x} H_{WD})]$	Two-gap correlation $\eta_r = 0.306$ (MSE = 0.0101)	Fit to Brody distribution $\eta = 0.0738$ (MSE = 0.241) (MSE = 0.000379)
	Poisson	Wigner-Dyson	Poisson	Wigner-Dyson			
⁶ Li	$\tilde{\chi}^2 = 0.760$ ($p = 0.582$)	$\tilde{\chi}^2 = 2.53$ ($p = 0.0435$)	$\tilde{G} = 0.982$ ($p = 0.436$)	$\tilde{G} = 2.08$ ($p = 0.0518$)	3.30		
⁷ Li	$\tilde{\chi}^2 = 1.40$ ($p = 0.246$)	$\tilde{\chi}^2 > 10^{10}$ ($p < 10^{-3}$)	$\tilde{G} = 0.760$ ($p = 0.654$)	$\tilde{G} = 8.06$ ($p < 10^{-11}$)	32.9	$\eta_r = 0.161$	$\eta = 0.241$ (MSE = 0.000379)

3. Erbium isotopic substitution

Erbium has five bosonic isotopes and the change in Li+Er reduced mass with respect to that of Li+¹⁶⁶Er is about $\pm 0.1\%$ for ^{6,7}Li. The small changes in μ , together with the nonchaotic nature and relatively low densities of the spectra all support and would simplify predicting the Feshbach spectra for different Er isotopes.

If δE_v is the isotopic shift in the binding energy of a near-dissociation molecular state and $\delta\mu_{\text{res}}$ is the difference between the magnetic moments of the molecule and free atoms (at resonance), the isotopic shift in resonance position, $\delta B_{\text{res}} \approx \delta E_v / \delta\mu_{\text{res}}$, may be estimated for an R^{-6} potential to be [67,68]

$$\delta B_{\text{res}} \approx \frac{3H_{6,1}^3}{2\delta\mu_{\text{res}}} (v_{D,1}^{\text{WKB}} - v)^2 \left(v + \frac{1}{2} \right) \left(1 - \frac{\mu_2}{\mu_1} \right), \quad (3)$$

where we approximated $\delta E_v \approx (dE_v/d\mu)|_{\mu_1} (\mu_2 - \mu_1)$. Both the parameter $H_{6,1} \approx 3.4346 \hbar (\mu_1 C_{6,0}^{1/3})^{-1/2}$ and the WKB noninteger quantum number at dissociation, $v_{D,1}^{\text{WKB}} = (1/\pi) \arctan(1 - a_{\text{bg},1}/\bar{a}_1) - 3/8$ —with $\bar{a}_1 \approx 0.47799 (2\mu_1 C_{6,0}/\hbar^2)^{1/4}$ —are calculated for a reference system. As expected, Eq. (3) shows that $\delta B_{\text{res}} > 0$ if $\mu_2 > \mu_1$, and vice versa ($\delta\mu_{\text{res}} < 0$ in our case). Equation (3) suggests that it may be possible to estimate the position of an equivalent resonance in a different isotopologue, while experiments may extract key information on background scattering lengths, quantum numbers, and nonadiabatic effects from isotopic resonance shifts.

4. Dependence on interaction potentials

It is not yet possible to calculate *quantitatively* correct *ab initio* Li+Er potentials, hence the robustness of our conclusions need to be assessed for their possible dependence on these. The energy of the top vibrational state may be estimated from the Van der Waals coefficient $C_{6,0}$ and reduced mass μ [69] to lie between 0 and $13 \hbar^2/(\mu R_{\text{vdW}}^2) \approx 6.3 \text{ h GHz}$ —where the characteristic length scale, $R_{\text{vdW}} = \frac{1}{2}(2\mu C_{6,0}/\hbar^2)^{1/4}$. The smallest difference between the magnetic moments of a scattering state and an $L = 0$ -supported bound state is μ_B . The largest magnetic field at which resonances from such levels might occur is thus $6.3 \text{ h GHz}/\mu_B \approx 5000 \text{ G}$. Resonances resulting from larger magnetic moment differences may appear at much lower fields; however, 5000 G is the smallest relevant range to study the dependence of our results on the interaction potentials.

Figure 4 shows a contour plot of the scattering length a for ⁷Li+¹⁶⁶Er as a function of the magnetic field, B , and a parameter λ used to scale the isotropic potentials, $V'_0 = \lambda V_0$.

To keep a practical computational cost, the calculations neglect hyperfine terms and use $L_{\text{max}} = 6$. The approximations preserve the main resonant features—compare with Fig. 2(b)—while the broadest resonances ($\Delta_B > 5 \text{ G}$) are most apparent at the grid's resolution. Fig. 4 reveals that there always exist broad magnetic Feshbach resonances at relatively low fields. Additionally, it shows that $\lambda = 1$ is statistically representative for a much wider λ range, except around 0.985 and 1.025 for which the background scattering length becomes very large and enhances all resonance widths.

IV. SUMMARY AND CONCLUSIONS

This work provides robust theoretical evidence that low-field magnetic Feshbach resonances immune to background losses exist for Li+Er, with widths $\Delta_B > 0.1$ well within current experimental resolution. Li+Er spectra are predicted to be nonchaotic, while remaining conveniently dense, in contrast with other systems involving highly-magnetic atoms such as Er+Er [32]. The predicted resonances may be resolved and independently addressed thus opening the door for precise tuning of Li+Er interactions and/or magnetoassociation into LiEr molecules. The characteristics of the spectra make it also possible to predict resonance positions for different isotopologues from measurements on a reference system, which would greatly simplify experiments with various Er isotopes and give key insight into nonadiabatic effects.

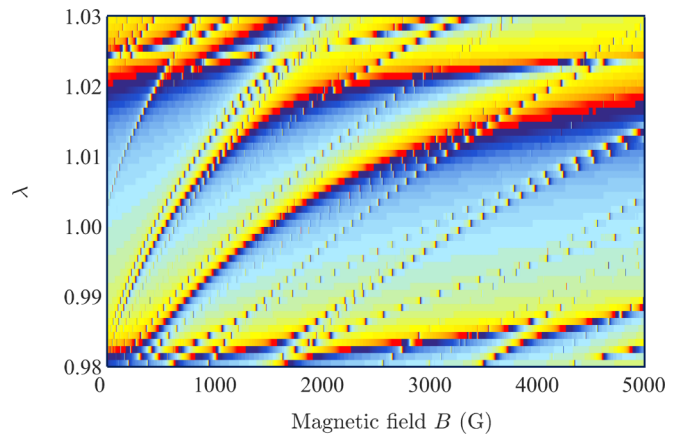


FIG. 4. (Color online) Contour plot of the scattering length a for ⁷Li+¹⁶⁶Er as a function of the magnetic field and a scaling parameter. Red (blue) indicates the highest (lowest) values.

ACKNOWLEDGMENTS

M.L.G.M. acknowledges funding from the European Community's Seventh Framework Programme (FP7/2007-2013) under Grant Agreement No. 330623. P.S.Ż. acknowl-

edges funding from the Polish National Science Center (NCN) grant DEC-2012/07/B/ST2/00235. This research is part of the French-Polish Scientific cooperation program POLONIUM.

-
- [1] L. D. Carr, D. DeMille, R. V. Krems, and J. Ye, *New J. Phys.* **11**, 055049 (2009).
 - [2] O. Dulieu and C. Gabbanini, *Rep. Prog. Phys.* **72**, 086401 (2009).
 - [3] I. Bloch, J. Dalibard, and S. Nascimbène, *Nat. Phys.* **8**, 267 (2012).
 - [4] M. A. Baranov, M. Dalmonte, G. Pupillo, and P. Zoller, *Chem. Rev.* **112**, 5012 (2012).
 - [5] A. Micheli, G. K. Brennen, and P. Zoller, *Nat. Phys.* **2**, 341 (2006).
 - [6] A. Micheli, G. Pupillo, H. P. Büchler, and P. Zoller, *Phys. Rev. A* **76**, 043604 (2007).
 - [7] H. P. Büchler, E. Demler, M. Lukin, A. Micheli, N. Prokof'ev, G. Pupillo, and P. Zoller, *Phys. Rev. Lett.* **98**, 060404 (2007).
 - [8] K.-K. Ni, S. Ospelkaus, D. Wang, G. Quéméner, B. Neyenhuis, M. H. G. de Miranda, J. L. Bohn, J. Ye, and D. S. Jin, *Nature (London)* **464**, 1324 (2010).
 - [9] S. Ospelkaus, K.-K. Ni, D. Wang, M. H. G. de Miranda, B. Neyenhuis, G. Quéméner, P. S. Julienne, J. L. Bohn, D. S. Jin, and J. Ye, *Science* **327**, 853 (2010).
 - [10] M. H. G. de Miranda, A. Chotia, B. Neyenhuis, D. Wang, G. Quéméner, S. Ospelkaus, J. L. Bohn, J. Ye, and D. S. Jin, *Nat. Phys.* **7**, 502 (2011).
 - [11] A. Derevianko and C. C. Cannon, *Phys. Rev. A* **70**, 062319 (2004).
 - [12] P. Rabl, D. DeMille, J. M. Doyle, M. D. Lukin, R. J. Schoelkopf, and P. Zoller, *Phys. Rev. Lett.* **97**, 033003 (2006).
 - [13] J. J. Hudson, B. E. Sauer, M. R. Tarbutt, and E. A. Hinds, *Phys. Rev. Lett.* **89**, 023003 (2002).
 - [14] T. Zelevinsky, S. Kotochigova, and J. Ye, *Phys. Rev. Lett.* **100**, 043201 (2008).
 - [15] B. J. Bloom, T. L. Nicholson, J. R. Williams, S. L. Campbell, M. Bishop, X. Zhang, W. Zhang, S. L. Bromley, and J. Ye, *Nature (London)* **506**, 71 (2014).
 - [16] C. Chin, R. Grimm, P. Julienne, and E. Tiesinga, *Rev. Mod. Phys.* **82**, 1225 (2010).
 - [17] J. M. Hutson and P. Soldán, *Int. Rev. Phys. Chem.* **25**, 497 (2006).
 - [18] T. Köhler, K. Góral, and P. S. Julienne, *Rev. Mod. Phys.* **78**, 1311 (2006).
 - [19] K. M. Jones, E. Tiesinga, P. D. Lett, and P. S. Julienne, *Rev. Mod. Phys.* **78**, 483 (2006).
 - [20] F. Lang, K. Winkler, C. Strauss, R. Grimm, and J. Hecker Denschlag, *Phys. Rev. Lett.* **101**, 133005 (2008).
 - [21] K.-K. Ni, S. Ospelkaus, M. H. G. de Miranda, A. Pe'er, B. Neyenhuis, J. J. Zirbel, S. Kotochigova, P. S. Julienne, D. S. Jin, and J. Ye, *Science* **322**, 231 (2008).
 - [22] J. G. Danzl, M. J. Mark, E. Haller, M. Gustavsson, R. Hart, J. Aldegunde, J. M. Hutson, and H.-C. Nägerl, *Nat. Phys.* **6**, 265 (2010).
 - [23] T. Takekoshi, L. Reichsöllner, A. Schindewolf, J. M. Hutson, C. R. Le Sueur, O. Dulieu, F. Ferlaino, R. Grimm, and H.-C. Nägerl, *Phys. Rev. Lett.* **113**, 205301 (2014).
 - [24] A. Griesmaier, J. Werner, S. Hensler, J. Stuhler, and T. Pfau, *Phys. Rev. Lett.* **94**, 160401 (2005).
 - [25] A. de Paz, A. Sharma, A. Chotia, E. Maréchal, J. H. Huckans, P. Pedri, L. Santos, O. Gorceix, L. Vernac, and B. Laburthe-Tolra, *Phys. Rev. Lett.* **111**, 185305 (2013).
 - [26] M. Lu, N. Q. Burdick, S. H. Youn, and B. L. Lev, *Phys. Rev. Lett.* **107**, 190401 (2011).
 - [27] M. Lu, N. Q. Burdick, and B. L. Lev, *Phys. Rev. Lett.* **108**, 215301 (2012).
 - [28] K. Aikawa, A. Frisch, M. Mark, S. Baier, A. Rietzler, R. Grimm, and F. Ferlaino, *Phys. Rev. Lett.* **108**, 210401 (2012).
 - [29] K. Aikawa, A. Frisch, M. Mark, S. Baier, R. Grimm, and F. Ferlaino, *Phys. Rev. Lett.* **112**, 010404 (2014).
 - [30] S. Kotochigova, *Rep. Prog. Phys.* **77**, 093901 (2014).
 - [31] A. Petrov, E. Tiesinga, and S. Kotochigova, *Phys. Rev. Lett.* **109**, 103002 (2012).
 - [32] A. Frisch, M. Mark, K. Aikawa, F. Ferlaino, J. L. Bohn, C. Makrides, A. Petrov, and S. Kotochigova, *Nature (London)* **507**, 475 (2014).
 - [33] K. Baumann, N. Q. Burdick, M. Lu, and B. L. Lev, *Phys. Rev. A* **89**, 020701(R) (2014).
 - [34] G. Quéméner and P. S. Julienne, *Chem. Rev.* **112**, 4949 (2012).
 - [35] B. Yan, S. A. Moses, B. Gadway, J. P. Covey, K. R. A. Hazzard, A. M. Rey, D. S. Jin, and J. Ye, *Nature (London)* **501**, 521 (2013).
 - [36] K. Aikawa, A. Frisch, M. Mark, S. Baier, R. Grimm, J. L. Bohn, D. S. Jin, G. M. Bruun, and F. Ferlaino, *Phys. Rev. Lett.* **113**, 263201 (2014).
 - [37] M. L. González-Martínez and J. M. Hutson, *Phys. Rev. A* **88**, 020701(R) (2013).
 - [38] Preliminary multireference configuration interaction (MRCI) calculations predict a permanent electric dipole moment of about 1.5 Debye for the lowest $^4\Sigma$ state, and the magnetic dipole moment may be up to approximately 8 Bohr magnetons.
 - [39] M. Tomza, *Phys. Rev. A* **88**, 012519 (2013).
 - [40] M. Tomza, *Phys. Rev. A* **90**, 022514 (2014).
 - [41] R. Pires, J. Ullmanis, S. Häfner, M. Repp, A. Arias, E. D. Kuhnle, and M. Weidemüller, *Phys. Rev. Lett.* **112**, 250404 (2014).
 - [42] M. L. González-Martínez and J. M. Hutson, *Phys. Rev. A* **88**, 053420 (2013).
 - [43] A. Beckmann, K. D. Böklen, and D. Elke, *Z. Phys.* **270**, 173 (1974).
 - [44] N. J. Stone, *At. Data Nucl. Data Tables* **90**, 75 (2005).
 - [45] W. C. Martin, R. Zalubas, and L. Hagan, *Atomic Energy Levels – The Rare Earth Elements*, National Standard Reference Data Series, Vol. 60 (National Bureau of Standards, Washington, 1978).

- [46] R. V. Krems, G. C. Groenenboom, and A. Dalgarno, *J. Phys. Chem. A* **108**, 8941 (2004).
- [47] H.-J. Werner, P. J. Knowles, G. Knizia, F. R. Manby, M. Schütz *et al.*, MOLPRO, version 2012.1: A package of *ab initio* programs (2012), <http://www.molpro.net>.
- [48] B. P. Prascher, D. E. Woon, K. A. Peterson, T. H. Dunning, Jr., and A. K. Wilson, *Theor. Chem. Acc.* **128**, 69 (2011).
- [49] M. Dolg, H. Stoll, and H. Preuss, *J. Chem. Phys.* **90**, 1730 (1989).
- [50] B. Jeziorski, R. Moszynski, and K. Szalewicz, *Chem. Rev.* **94**, 1887 (1994).
- [51] P. Zhang, H. R. Sadeghpour, and A. Dalgarno, *J. Chem. Phys.* **133**, 044306 (2010).
- [52] W. Heisenberg, *Z. Phys.* **49**, 619 (1928).
- [53] A. A. Buchachenko, G. Chałasiński, and M. M. Szczęśniak, *J. Chem. Phys.* **131**, 241102 (2009).
- [54] T. V. Tscherbul, J. Kłos, A. Dalgarno, B. Zygelman, Z. Pavlovic, M. T. Hummon, H.-I. Lu, E. Tsikata, and J. M. Doyle, *Phys. Rev. A* **82**, 042718 (2010).
- [55] T.-S. Ho and H. Rabitz, *J. Chem. Phys.* **104**, 2584 (1996).
- [56] K. T. Tang, *Phys. Rev.* **177**, 108 (1969).
- [57] A. Derevianko, S. G. Porsev, and J. F. Babb, *At. Data Nucl. Data Tables* **96**, 323 (2010).
- [58] M. Lepers, J.-F. Wyart, and O. Dulieu, *Phys. Rev. A* **89**, 022505 (2014).
- [59] X. Chu, A. Dalgarno, and G. C. Groenenboom, *Phys. Rev. A* **75**, 032723 (2007).
- [60] R. V. Krems, J. Kłos, M. F. Rode, M. M. Szczęśniak, G. Chałasiński, and A. Dalgarno, *Phys. Rev. Lett.* **94**, 013202 (2005).
- [61] A. A. Buchachenko, G. Chałasiński, and M. M. Szczęśniak, *Eur. Phys. J. D* **45**, 147 (2007).
- [62] J. M. Hutson and S. Green, computer code MOLSCAT, version 14, CCP6, Daresbury (1994).
- [63] M. L. González-Martínez and J. M. Hutson, *Phys. Rev. A* **75**, 022702 (2007).
- [64] J. M. Hutson, computer code FIELD, version 1 (2011).
- [65] D. J. C. MacKay, *Information Theory, Inference, and Learning Algorithms* (Cambridge University Press, London, 2003).
- [66] A. C. A. Hope, *J. R. Stat. Soc. Ser. B* **30**, 582 (1968).
- [67] R. J. LeRoy and R. B. Bernstein, *J. Chem. Phys.* **52**, 3869 (1970).
- [68] G. F. Gribakin and V. V. Flambaum, *Phys. Rev. A* **48**, 546 (1993).
- [69] B. Gao, *J. Phys. B: At. Mol. Opt. Phys.* **37**, 4273 (2004).